

NFL-BA: Improving Endoscopic SLAM with Near-Field Light Bundle Adjustment

Andrea Dunn Beltran^{*}, Daniel Rho^{*}, Marc Niethammer, Roni Sengupta
University of North Carolina at Chapel Hill

^{*} Equal contribution

{asdunnbe, dn103c1, mn, ronisen}@cs.unc.edu

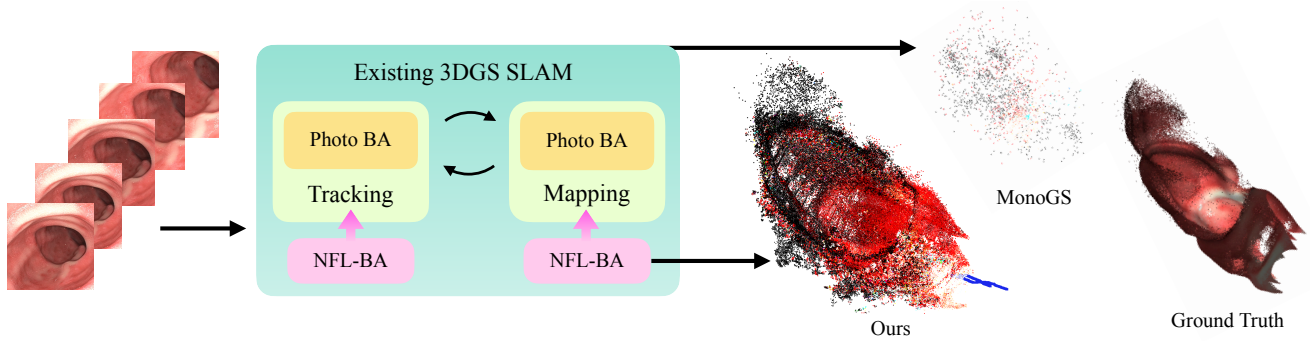


Figure 1. We introduce Near-Field Light Bundle Adjustment (NFL-BA) which can significantly improve the tracking and mapping performance of existing 3D Gaussian-based SLAM algorithms, e.g. MonoGS SLAM, on endoscopy videos that exhibit significant dynamic near-field lighting with textureless surfaces and specular reflections. Our camera trajectory is shown in blue, the color of point clouds are obtained from the Gaussians without opacity values - red and black indicates large and small intensity of incident light.

Abstract

Simultaneous Localization And Mapping (SLAM) from a monocular endoscopy video can enable autonomous navigation, guidance to unsurveyed regions, and 3D visualizations, which can significantly improve endoscopy experience for surgeons and patient outcomes. Existing dense SLAM algorithms often assume distant and static lighting and textured surfaces, and alternate between optimizing scene geometry and camera parameters by minimizing a photometric rendering loss, often called Photometric Bundle Adjustment. However, endoscopic environments exhibit dynamic near-field lighting due to the co-located light and camera moving extremely close to the surface, textureless surfaces, and strong specular reflections due to mucus layers. When not considered, these near-field lighting effects can cause significant performance reductions for existing SLAM algorithms from indoor/outdoor scenes when applied to endoscopy videos. To mitigate this problem, we introduce a new Near-Field Lighting Bundle Adjustment Loss (\mathcal{L}_{NFL-BA}) that can also be alternately optimized, along with the Photometric Bundle Adjustment loss, such that the captured images' intensity

variations match the relative distance and orientation between the surface and the co-located light and camera. We derive a general NFL-BA loss function for 3D Gaussian surface representations and demonstrate that adding \mathcal{L}_{NFL-BA} can significantly improve the tracking and mapping performance of two state-of-the-art 3DGS-SLAM systems, MonoGS (35% improvement in tracking, 48% improvement in mapping with predicted depth maps) and EndoGSLAM (22% improvement in tracking, marginal improvement in mapping with predicted depths), on the C3VD endoscopy dataset for colons. The project page is available at <https://asdunnbe.github.io/NFL-BA/>

1. Introduction

Simultaneous Localization and Mapping (SLAM) is commonly used by autonomous systems to create a map of an unknown environment while simultaneously determining their own location within it, with applications in Computer Vision, Robotics, and Medical Imaging. SLAM systems often consider various surface representations, e.g. point clouds [30, 32], 3D Gaussians [15, 18, 26, 45], and neural representations [4, 56, 59, 61], and alternate between optimizing camera tracking and mapping. For dense SLAM

systems, every pixel is often tracked using a Photometric Bundle Adjustment, where camera parameters and surface representations are alternately optimized to minimize the 3D-to-2D photometric projection error.

Recently, researchers have explored the effectiveness of SLAM to enable autonomous or assistive endoscopy procedures, where a slender flexible tube with a co-located light and camera is used to inspect internal organs such as the lungs and colons [7, 16, 23, 29, 48, 53]. SLAM can enable autonomous navigation through internal organs, guide surgeons to unsurveyed regions, improve surgeons’ situational awareness by providing 3D visualizations, and can help measure organ shapes, e.g. the cross-sectional area of the upper airway to diagnose airway abnormalities [51].

However, endoscopic environments create unique challenges that significantly reduce the performance of conventional SLAM algorithms. Unlike typical scenes where illumination is distant and approximately uniform, endoscopic procedures involve a moving light source co-located with the camera close to the tissue surface. This causes dynamic near-field lighting effects, where at each time different points of the surface receive different intensities of light depending on the distance and orientation of the point to the camera. In addition, tissue surfaces often contain minimal textures, exhibit strong specular reflections, and cast shadows due to the presence of ridges on the surface, all of which negatively impact feature extraction and matching [9, 19]. Thus, existing Photometric and Geometric Bundle Adjustment (BA) losses, which often assume static distant lighting conditions, suffer in endoscopic applications of SLAM due to strong near-field lighting and specular reflections creating intensity shifts across frames that distort photometric and geometric correspondences, resulting in poor tracking and mapping performance.

To alleviate these issues, we create a new Bundle Adjustment loss that accounts for dynamic near-field lighting. Our key intuition is that the captured image and its lighting effects can provide valuable information about the relative distance and orientation between each point on the surface and the camera, e.g. the point closest to the camera with the surface normal towards the camera will receive large incoming light and hence will have a larger intensity value in the captured image compared to points that are further away from the camera or with surface normals pointing away from the camera. With this intuition, we formulate a Near-Field Lighting Bundle Adjustment loss (\mathcal{L}_{NFL-BA}) where we can alternate between optimizing the surface geometry and camera parameters such that the rendered image has intensity variations that match the relative distance and orientation between the surface and the camera.

Inspired by the recent success of 3D Gaussian Splatting in SLAM [33], we define the Near-Field Lighting Bundle Adjustment loss (\mathcal{L}_{NFL-BA}) for 3D Gaussian surface rep-

resentations. We then consider two state-of-the-art 3DGS-based SLAM systems, MonoGS [24] and EndoGSLAM [53], and show that adding our proposed Near-Field Lighting Bundle Adjustment loss (\mathcal{L}_{NFL-BA}) in their Tracking and Mapping components can significantly improve their performance on a commonly used phantom colonoscopy dataset C3VD [2]. For example, with depth initialized by a state-of-the-art monocular depth estimator PPSNet [31], \mathcal{L}_{NFL-BA} significantly improves camera localization for MonoGS by 35% and for EndoGSLAM by 22%, and image rendering perceptual quality (LPIPS metric) for MonoGS by 48% and marginally for EndoGSLAM.

2. Related Works

Dense SLAM. While early SLAM systems relied on feature matching approaches [3, 10, 27, 37], with advancements in neural implicit representations and novel encoding techniques, recent SLAM frameworks [60, 62] can improve robustness and details in mapping and tracking. Recently 3D Gaussian surface representation with differentiable rasterization in SLAM framework [8, 15, 18, 26, 45, 50] demonstrated real-time rendering while enhancing mapping accuracy. We also consider 3DGS-SLAM frameworks for developing and demonstrating the effectiveness of Near-Field Light Bundle Adjustment loss.

SLAM in endoscopy. SLAM systems tailored for endoscopy confront unique challenges due to dynamic near-field lighting, textureless surfaces, strong specular highlights, deformable tissues, and complex endoscope motion, which deteriorate the performance of SLAM systems that rely only on photometric feature matching. Attempts to model tissue deformation as non-rigid surface reconstruction [6, 11, 22, 35, 36, 43, 46, 52] generally consider small camera motion, i.e. laparoscopy procedures, which is not the focus of this paper. Researchers have often used a mixture of supervised learning on synthetic and self-supervised learning on real endoscopy datasets for adapting SLAM frameworks to endoscopy with complex camera motion [25, 34, 42, 55]. Gaussian-splatting-based methods [12, 14, 23, 40, 48] proved especially effective due to its fast rendering speed, ability to generate high-quality details and model textureless regions with a large number of Gaussians. Hence we also adopt 3D Gaussian Splatting-based SLAM approaches and explicitly model the near-field lighting effects as a Bundle Adjustment loss, which alleviates dynamic near-field lighting challenges and improves tracking of textureless regions with lighting-based cues while ignoring specular highlights.

Bundle Adjustment in SLAM. Bundle Adjustment (BA) alternatively optimizes camera parameters and surface geometry by minimizing errors across multiple frames. Traditional geometric Bundle Adjustment minimizes reprojection error by aligning salient 2D image points with corresponding 3D points, assuming static lighting and Lamber-

tian surfaces [13]. While effective in controlled environments, it struggles in complex or low-texture scenes like endoscopy. Photometric Bundle Adjustment [1] incorporates pixel intensities into the optimization process, minimizing photometric re-projection errors and proving advantageous in texture-poor environments where feature matching fails [10]. Recent advancements integrate learned feature representations to handle photometric variations in dynamic lighting, enhancing robustness in complex environments [58]. However, Photometric Bundle Adjustment does not exploit the correspondence cues provided by near-field lighting, i.e. image intensity varies with the relative distance and orientation between the surface point and the camera, which we formulate as Near-Field Light Bundle Adjustment and demonstrate its effectiveness in improving the performance of SLAM frameworks on endoscopic scenes.

Near-field Lighting models. Near-field lighting has been leveraged for 3D reconstruction tasks like monocular depth and surface normal estimation [31, 57] and Photometric Stereo [20]. Some of these approaches [20, 31] use a near-field lighting representation, similar to ours, as input to a CNN along with captured images for predicting surface normal and geometry. In the context of Endoscopy, PPSNet [31] demonstrated the effectiveness of near-field lighting to enhance monocular depth estimation by introducing a supervised and a self-supervised loss function that derives a per-pixel shading field and calculates its similarity with the captured image. Researchers have often formulated image formation models with multiple light sources in the endoscope and solved a Shape from Shading [57] or Structure from Motion [39], often in simulation environments. In contrast, we propose a Bundle Adjustment Loss with Near-Field Lighting (NFL-BA), considering the most commonly available single co-located camera & light in the endoscope. NFL-BA can improve the performance of any 3D Gaussian-based SLAM framework for realistic colon data, which has not been done before, to our knowledge.

3. Method

We introduce a novel Near-Field Lighting based Bundle Adjustment loss, \mathcal{L}_{NFL-BA} , which is used to alternate between optimizing camera pose and 3D surface representation in a SLAM framework, along with the commonly used Photometric re-rendering-based Bundle Adjustment loss. While our proposed loss function is general, in this work we focus on 3D Gaussian Splatting-based SLAM frameworks [26, 53], which performs best for both indoor and endoscopic scenes compared to sparse or dense point clouds and neural implicit surface representations. In Sec. 3.1 we first introduce the general principle of SLAM with 3D Gaussian Splatting. Then in Sec. 3.2 we introduce the photometric image formation model for near-field lighting. While this image formation model has been well established [21] and

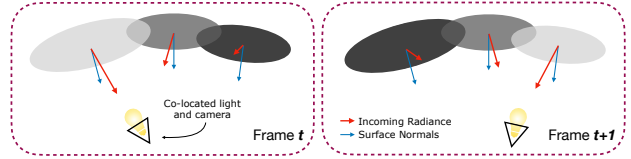


Figure 2. Illustration of our key idea. As the endoscope, with a co-located light and camera, moves through the scene, different 3D Gaussians on the surface receive different intensities of light (red arrow), dependent on the relative distance and orientation between the 3D Gaussian and the camera. Building on this idea, we develop a novel Near-Field Light Bundle Adjustment loss that optimizes camera pose and 3D Gaussian parameters to align the computed light intensity with the actual pixel intensity.

has often been used as input to Photometric Stereo neural networks [21] and within the loss function for training Monocular Depth Estimation algorithms [31], it has never been used for Simultaneous Localization & Mapping (SLAM) or Structure from Motion (SfM) problems, let alone in combination with 3D Gaussian Splatting. In Sec. 3.3 we formulate NFL-BA and in Sec. 3.3 we discuss how two state-of-the-art SLAM algorithms, MonoGS-SLAM [26] and EndoGS-SLAM [53] can be improved by using \mathcal{L}_{NFL-BA} .

3.1. SLAM with Gaussian Splatting

Let us denote camera extrinsic parameters at time t as $T_t = [R_t, C_t] \in \mathbf{SE}(3)$, where R_t and C_t are the rotation and translation for the world to camera transformation, and projection matrix $\pi_t = K T_t$, where K describes the camera intrinsic parameters which we assume to be same for all frames, and which are often known or calibrated ahead of time. Let us denote parameters for representing a given scene as Θ . Based on 3D Gaussian Splatting [18], we consider the scene to be represented with a set of Gaussians $\Theta = \{\mathcal{G}^i\}$ and their parameters: the mean μ^i , the covariance Σ^i in the world space, and the optical properties consisting of the color c^i and the opacity α^i . We can calculate the shape parameters and opacities of the *splatted* 2D Gaussians as follows:

$$\begin{aligned} \bar{\mu}_t^i &= \pi_t \mu^i, & \bar{\Sigma}_t^i &= J_t R_t \Sigma^i R_t^T J_t^T, \\ \bar{\alpha}_t^i &= \alpha^i \exp\left(-\frac{1}{2}(p - \bar{\mu}_t^i)^\top (\bar{\Sigma}_t^i)^{-1} (p - \bar{\mu}_t^i)\right), \end{aligned} \quad (1)$$

where J_t is the Jacobian of the linear approximation of the projective transformation π_t and p is a coordinate in the pixel space. $\bar{\mu}_t^i$ and $\bar{\Sigma}_t^i$ are the splatted mean and covariance of a Gaussian \mathcal{G}^i in the pixel space.

Given camera parameters, one first sorts all Gaussians by distance from the camera (from near to far) and then renders an RGB image by alpha-compositing the splatted 2D Gaussians in pixel space. Specifically, we render the color $\tilde{C}_t(\cdot)$

and depth $\hat{D}_t(\cdot)$ of a pixel p from a frame at time t using:

$$\begin{aligned}\hat{C}_t(p) &= \sum_{i \in \mathcal{N}} c^i \bar{\alpha}_t^i \prod_{j=1}^{i-1} (1 - \bar{\alpha}_t^j), \\ \hat{D}_t(p) &= \sum_{i \in \mathcal{N}} z^i \bar{\alpha}_t^i \prod_{j=1}^{i-1} (1 - \bar{\alpha}_t^j),\end{aligned}\quad (2)$$

where \mathcal{N} denotes the set of 2D Gaussians that overlap for a pixel p , indexing i is from near to far, z^i is the z coordinate of the center (mean) of the 3D Gaussian after transforming from world to the t -th camera coordinate space.

SLAM with 3D Gaussian surface representation often minimizes a Photometric Bundle Adjustment loss where a rendered image is compared to a captured image [24, 45]. This loss often includes an additional term that compares the rendered depth map with a depth map predicted by a monocular depth estimation algorithm or measured with a RGBD sensor [38]. Thus we can define a generic Photometric bundle adjustment loss as:

$$\begin{aligned}\mathcal{L}_{photo-BA} &= \mathcal{L}_{rgb}(\hat{C}_t, C_t; M_t) \\ &+ \lambda_{depth} \mathcal{L}_{depth}(\hat{D}_t, D_t; M_t),\end{aligned}\quad (3)$$

where M_t is a pixel-wise weighting map often used to handle visibility or over and under-saturated pixels. C_t and \hat{C}_t denote the target image and the rendered image, respectively. Similarly, D_t and \hat{D}_t are target and rendered depth maps, if given. λ_{depth} is a weight balancing between the image and the depth re-rendering loss, which can be non-zero when measured depth from a RGBD sensor is available. The color loss \mathcal{L}_{rgb} and depth loss \mathcal{L}_{depth} are usually P -Norm-based loss functions, e.g. $\mathcal{L}_{rgb}(\hat{C}_t, C_t; M_t) = \sum_p M_t(p) \cdot \|\hat{C}_t(p) - C_t(p)\|_P$, but they can vary depending on the optimization strategies.

Most SLAM pipelines involve a tracking and a mapping part where camera pose and 3D surface representations are optimized separately using:

$$\begin{aligned}\text{Tracking: } & \min_{T_t} \sum_t \mathcal{L}_{photo-BA} + \lambda_{reg} \mathcal{L}_{reg}, \\ \text{Mapping: } & \min_{\Theta} \sum_t \mathcal{L}_{photo-BA} + \lambda_{reg} \mathcal{L}_{reg},\end{aligned}\quad (4)$$

where \mathcal{L}_{reg} is a regularization loss with hyperparameter λ_{reg} . Depending on optimization algorithms, the pose-related parameters T_t might be additionally included during mapping optimization. Different SLAM systems often apply different variations of the Photometric Bundle Adjustment depending on the goal and the application.

3.2. Image Formation with Near-Field Lighting

We consider an image-formation model with near-field lighting for a single image following previous descriptions

[17, 31]. Then each three-dimensional point X on the surface and its corresponding pixel location p receives different light intensities and directions, characterized by light direction $L^d(p)$ and attenuation $L^a(p)$, as follows:

$$L^d(p) = \frac{C_t - X(p)}{d(p)}, \quad L^a(p) = \frac{(L^d(p)^\top r_t^e)^\beta}{d(p)^2}, \quad (5)$$

where $d(\cdot)$ is a depth map, which can be obtained as $d(p) = \|C_t - X(p)\|$ or by directly using the rendered depth map $\hat{D}_t(\cdot)$ (Eq. 2). r_t^e is the direction of light which is the primary axis of the camera that points towards the surface and can be obtained by converting the camera rotation matrix to an axis-angle representation $R_t = (r_t^e, r_t^\theta)$, and β is an angular attenuation coefficient.

As the diffuse reflectance model has been useful for depth estimation in endoscopic scenes [31], we also assume direct illumination with a diffuse reflectance model. We can approximate the rendered image at each pixel $\hat{I}(p)$ as:

$$\hat{I}(p) \approx \rho(p) \cdot L^a(p) \cdot (L^d(p)^\top N(p)), \quad (6)$$

where $\rho(p)$ and $N(p)$ are albedo and surface normal at pixel p respectively.

3.3. Near-Field Lighting Bundle Adjustment Loss

Next, we introduce a Bundle Adjustment loss function using the near-field light image formation model. Our key intuition is that the image formation with near-field light defined in Eq. 6 can provide information for the scene geometry and camera pose updates. More specifically, the scene geometry influences the formed image through the normal vector $N(p)$ and the distance $d(p)$, while the camera location and rotation along with the distance $d(p)$ affect the lighting direction $L^d(p)$ and attenuation $L^a(p)$ terms. Thus optimizing a loss function derived from this image formation model can enable better optimization for both camera pose and scene geometry.

As for normal maps, we can calculate normals from mapping parameters Θ or extract them from generated depth maps using Θ . We first calculate the normals on the 3D Gaussians as the direction of the shortest axis of the Gaussian following [5, 44, 49]. Specifically, we calculate the eigendecomposition of Σ^i and the eigenvector corresponding to the smallest eigenvalue represents the surface normal N^i as: $N^i = V_j^i$, where $j = \arg \min \text{diag}(\Lambda^i)$ and $\Sigma^i = V^i \Lambda^i (V^i)^{-1}$.

We can then transform the 3D Gaussian normals from world to camera coordinates using the rotation matrix R_t and then splat it to pixel space using alpha blending, similar to how the depth map and color are computed in Eq. 2, using the following equation:

$$\hat{N}_t(p) = \sum_{i \in \mathcal{N}} (R_t N^i) \alpha_t^i(p) \prod_{j=1}^{i-1} (1 - \alpha_t^j(p)). \quad (7)$$

| Method | Depth | \mathcal{L}_{NFL-BA} | Tracking | | Mapping | Rendering | | | |
|-----------|-------------|------------------------|-------------------------|--------------------|-------------|--------------|-------------|-------------|-------------|
| | | | ATE _t (mm) ↓ | ATE _r ↓ | Chamfer ↓ | PSNR ↑ | RMSE ↓ | SSIM ↑ | LPIPS ↓ |
| MonoGS | - | ✗ | 2.33 | 1.13 | 1.60 | 18.78 | 0.14 | 0.72 | 0.46 |
| | - | ✓ | 2.31 | 1.53 | 1.74 | 18.80 | 0.13 | 0.72 | 0.47 |
| | DA2 [47] | ✗ | 5.31 | 2.49 | 3.43 | 18.69 | 0.13 | 0.69 | 0.64 |
| | DA2 [47] | ✓ | 4.88 | 2.35 | 1.71 | 17.73 | 0.14 | 0.68 | 0.59 |
| | PPSNet [31] | ✗ | 3.72 | 1.65 | 3.72 | 19.03 | 0.12 | 0.71 | 0.56 |
| | PPSNet [31] | ✓ | 2.40 | 1.98 | 0.71 | 20.60 | 0.10 | 0.66 | 0.43 |
| | oracle | ✗ | 3.20 | 1.48 | 1.27 | 19.73 | 0.12 | 0.73 | 0.51 |
| | oracle | ✓ | 1.72 | 1.36 | 0.68 | 19.55 | 0.13 | 0.74 | 0.37 |
| EndoGSLAM | DA2 [47] | ✗ | 7.27 | 2.32 | 6.35 | 10.00 | 0.34 | 0.33 | 0.61 |
| | DA2 [47] | ✓ | 6.26 | 2.15 | 5.68 | 12.37 | 0.26 | 0.44 | 0.56 |
| | PPSNet [31] | ✗ | 3.16 | 1.72 | 1.12 | 17.26 | 0.16 | 0.63 | 0.39 |
| | PPSNet [31] | ✓ | 2.48 | 1.68 | 1.32 | 17.92 | 0.14 | 0.63 | 0.38 |
| | oracle | ✗ | 1.68 | 1.80 | 0.81 | 18.40 | 0.13 | 0.65 | 0.36 |
| | oracle | ✓ | 1.55 | 1.71 | 0.81 | 18.66 | 0.13 | 0.65 | 0.35 |

Table 1. Quantitative Evaluation on 8 sequences from the C3VD [2]. Our proposed Near-Field Light Bundle Adjustment (NFL-BA) significantly improves tracking, mapping and rendering quality of two state-of-the-art 3D Gaussian SLAMs for different depth inputs.

For calculating the 3D point X for a pixel p , we can use the following equation:

$$X_t(p) = \hat{D}_t(p)K^{-1}[p, 1]^T. \quad (8)$$

Finally, we can combine the surface normal representation in Eq. 7 and the 3D point calculation in Eq. 8, to update the image formation model of Eq. 6. Based on these, we propose a scale-invariant Near-Field Lighting Bundle Adjustment loss as follows:

$$\mathcal{L}_{NFL-BA} = \min_s \sum_p M_t(p) \cdot (\|I_t(p) - s \cdot \hat{\rho}_t(p) \cdot L_t^\alpha(p) \cdot (L_t^d(p)^\top \hat{N}_t(p))\|_2), \quad (9)$$

where $\hat{\rho}_t(p)$ is the albedo which is also in linear RGB space, $M_t(p)$ is a binary mask that is set to 0 for highly specular regions and 1 otherwise, helps to remove pixels from the loss computation that do not follow the diffuse near-field image formation model. Lastly, s is a scaling factor for a scale-invariant L_2 loss by calculating the optimal scale s that minimizes the loss, which is needed since the exact intensity of the light source is unknown.

We then incorporate this loss in both the tracking and the mapping parts of a SLAM approach and update Eq. 4 as:

$$\begin{aligned} \text{Tracking: } & \min_{T_t} \sum_t \mathcal{L}_{photo-BA} + \lambda_{NFL} \mathcal{L}_{NFL-BA}, \\ \text{Mapping: } & \min_{\Theta} \sum_{t \in K} \mathcal{L}_{photo-BA} + \lambda_{NFL} \mathcal{L}_{NFL-BA}. \end{aligned} \quad (10)$$

We ignore the regularization loss \mathcal{L}_{reg} for brevity and λ_{NFL} is a hyperparameter controlling the importance of our proposed Near-Field Lighting Bundle Adjustment loss.

3.4. Implementation Details

Our implementation of the \mathcal{L}_{NFL-BA} loss involves several practical adjustments to the theoretical model to ensure computational

efficiency and robustness in real-world scenarios. Following previous works [21, 31], we simplify the near-field light image formation model by setting the attenuation coefficient β in Eq. 5 to zero. This effectively ignores the directional fall-off component, reducing the light attenuation term to a simple inverse-square fall-off $L^\alpha(p) = 1/\|C_t - X(p)\|^2$. This simplification is justified because the angular attenuation in endoscopic imaging is often negligible compared to the inverse square law attenuation, and estimating β accurately can be challenging due to variations in endoscope designs. In future work, we plan to empirically determine the optimal value of β for specific endoscopic systems and incorporate the light direction vector r_t^e for more accurate modeling which can further improve camera rotation during Bundle Adjustment.

To focus on regions where the near-field lighting model is most accurate and to mitigate the effects of lens vignetting and peripheral distortions, we crop the images to their central regions when computing \mathcal{L}_{NFL-BA} . This cropping acts as a form of spatial weighting, effectively ignoring areas where the lighting model may not hold due to significant angular deviations. By concentrating on the central area, we ensure that the loss computation is based on pixels with more consistent illumination.

Albedo was estimated by converting each RGB image to HSV color space, setting the value channel to 1 across all pixels, and subsequently converting the modified image back to RGB space. This method standardizes pixel intensity variations, approximating a reflectance map where illumination effects are minimized, though it does not strictly represent ground truth albedo. It provides a relative albedo estimate that assumes uniform surface reflectance under consistent lighting conditions. Both the captured image $I_t(p)$ and the estimated albedo $\hat{\rho}_t(p)$ are converted to linear RGB space using gamma correction with $\gamma = 2.2$, ensuring consistency with the assumed linearity in the image formation model.

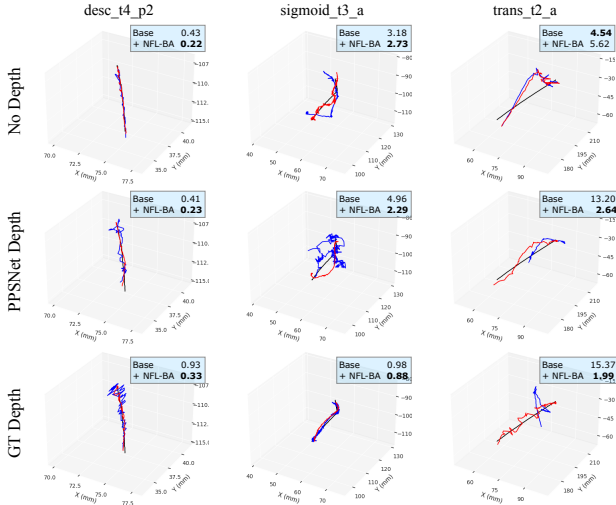


Figure 3. Camera tracking improvement over MonoGS [24]. We show that the proposed NFL-BA loss (in blue) improves the tracking of the baseline SLAM algorithm, MonoGS (in red), for 3 sequences for different depth initialization. Average tracking error ATE_t for each sequence is reported in the inset (zoom for details).

4. Evaluation

Our proposed method can be applied to any existing SLAM framework, especially one that uses 3D Gaussian surface representations. We test our Near-Field Lighting based Bundle Adjustment loss \mathcal{L}_{NFL-BA} on both general purposed, MonoGS-SLAM [26] and Endoscopy-specific method, EndoGSLAM [53].

4.1. Evaluation Setting

Dataset. We evaluate our proposed method using the Colonoscopy 3D Video Dataset (C3VD) [2], which provides paired depth data from 2D-3D registration in colonoscopic videos. The dataset features high-resolution RGB images coupled with corresponding depth maps, capturing the intricate geometry and challenging near-field lighting conditions inherent to endoscopic procedures. The C3VD dataset was created using a phantom colon with synthetic materials to simulate realistic tissue geometry. The endoscopy video was captured by a surgeon who performs different endoscopy procedures on the phantom colon with a real endoscope, resulting in realistic camera trajectories mimicking actual operative procedures. The phantom colon model is segmented into five main regions: the sigmoid colon, descending colon, transcending colon, ascending colon, and cecum. As depth information might not be available for every endoscope, we test our proposed method with or without ground truth depth maps. We also run experiments with depth maps from an off-the-shelf monocular depth estimator, as the estimated depth maps can help understand the structure better even without ground truth depths [47]. As for the depth estimator, we use PPSNet [31], a state-of-the-art monocular depth estimation algorithm for endoscopy. For comparison, we also use a state-of-the-art general-purpose depth estimator, Depth Anything v2 [47]. We test our method on a subset of 8 videos with at least one video from each section of the colon, with varying camera motion, and anomalies, such as polyps as shown

in Fig. 5. These eight videos belong to the test dataset of PPSNet [31], which we use for initializing depth maps in SLAM frameworks. Detailed information on our dataset split can be found in the supplementary materials. All images were cropped to remove any artifacts resulting from fish-eye correction.

Baselines. In our experiments, we evaluate the effectiveness of our proposed NFL-BA loss function by integrating it into the two existing SLAM systems: MonoGS [24] and EndoGSLAM [53].

MonoGS [24] is a monocular SLAM algorithm that employs bundle adjustment in both tracking and mapping. During the tracking phase, MonoGS optimizes camera parameters over all frames, while during the mapping phase, it optimizes both 3D Gaussian parameters and camera pose using Photometric Bundle Adjustment loss. While MonoGS was originally proposed as an RGB and RGB-D SLAM framework for indoor scenes, we can train it for endoscopy videos using three different depth input settings: without any depth input, with noisy estimated depth inputs from a monocular depth estimation algorithm [31], and with ground truth or oracle depth input. For each of these depth input settings, we train MonoGS with and without Near-Field Light Bundle Adjustment loss \mathcal{L}_{NFL-BA} to demonstrate SLAM performance improvement across different conditions. In a true monocular setting, we only incorporate \mathcal{L}_{NFL-BA} into the mapping phase with a weight of 0.5. In the estimated depth map setting, we set both tracking and mapping weights to 0.001. Additionally, since estimated depth maps are noisy, we set the λ_{depth} to 0.4 to account for the noise. We set the weights of our loss for GT depth to 0.001 and 0.001 for tracking and mapping respectively.

EndoGSLAM [53] is a RGB-D SLAM that works similarly to MonoGS [24] but is specifically engineered for endoscopic settings. We train EndoGSLAM by initializing depth with both oracle depth and depth map predicted by PPSNet [31], and train it with and without our proposed loss \mathcal{L}_{NFL-BA} . We set the weights of both mapping and tracking weights to 0.01 in the PPSNet Depth setting. For RGB-D setting, we used 0.001 and 0.005 for tracking and mapping loss weights, respectively.

Metrics. We follow other 3D Gaussian SLAM algorithms [24, 53] and evaluate the tracking performance using the root mean square error across all frames of Absolute Trajectory Error in translation ATE_t , measured in millimeters, and Absolute Trajectory Error in rotation ATE_r , measured in degrees to evaluate the accuracy of the estimated camera trajectory. Similarly, we also assess mapping quality by re-rendering images. We follow the default evaluation settings for each SLAM baseline, for EndoGSLAM, we calculate the rendering error of held-out frames, but for MonoGS, we evaluate the performance on the keyframe, which is a subset of training frames. We measure the quality of the rendered image by using the Peak Signal-to-Noise Ratio (PSNR) and the Learned Perceptual Image Patch Similarity (LPIPS) [54], commonly used in 3D Gaussian Splatting-based SLAM systems [24, 33]. To measure the mapping quality, we use point cloud-based evaluation. As there are no ground truth point clouds, we unproject 2D images into 3D space with the correct camera configuration and the oracle depth maps. For SLAM systems, we use the centers of Gaussians after optimization. For point cloud alignment, we use Coherent Point Drift [28]. To measure the quality of point clouds, we use the Chamfer distance from ground truth to the nearest points in the estimated point clouds [41]. As for absolute trajectory error in

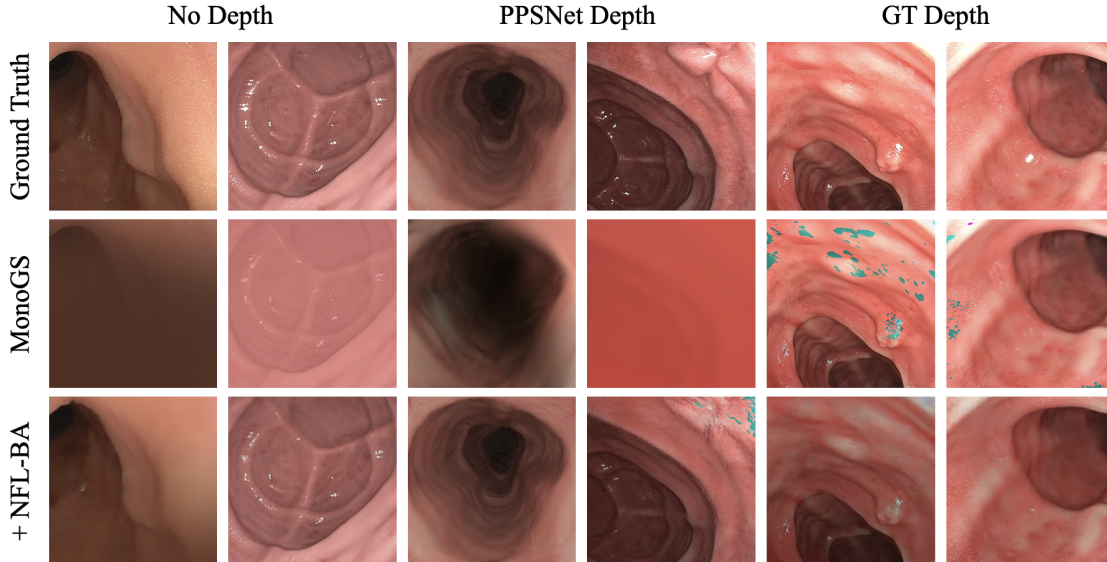


Figure 4. Mapping improvement over MonoGS with different depth inputs. The first two columns are from the monocular setting, the following two columns are from the estimated depths setting, and the last two are from the RGB-D setting.

translation ATE_t , Chamfer distances are in millimeters.

4.2. Improving MonoGS with NFL-BA

Tracking. As Table 1 shows, the integration of \mathcal{L}_{NFL-BA} significantly improves tracking accuracy in the MonoGS system across both oracle and estimated depth initialization, though the benefits are marginal in the no-depth initialization setting. Without \mathcal{L}_{NFL-BA} , the baseline MonoGS configuration with PPSNet-generated depth initialization produces a somewhat high ATE_t , highlighting the challenges faced when only noisy, estimated depth is available to SLAM. When \mathcal{L}_{NFL-BA} is applied, the performance improves considerably and reduces ATE_t by approximately 35%. This notable improvement in tracking accuracy suggests that our proposed loss effectively mitigates the impact of noisy depth by accounting for near-field lighting variations, resulting in more reliable camera pose estimations in challenging conditions (Table 1). In the oracle or ground-truth depth initialization, while MonoGS performs well with accurate depth data, NFL-BA provides additional benefits in aligning feature correspondences and reducing trajectory errors as seen in Fig. 3 and Tab. 1.

Mapping. Mapping accuracy, assessed through Chamfer distance, benefits from the integration of \mathcal{L}_{NFL-BA} across different depth inputs. We saw that the inclusion of \mathcal{L}_{NFL-BA} led to more dense, complete point clouds. As seen in Figs. 7 and 9, the point clouds are also more structurally similar to the ground truth input. For both ground truth and estimated depth maps, the mapping performance improves by approximately 50% to 80%, measured in Chamfer distance.

Rendering. When comparing configurations with and without the \mathcal{L}_{NFL-BA} loss, there is a marked improvement in rendering metrics, specifically in PSNR and LPIPS scores, indicating enhanced perceptual similarity to the original images and reduced error. As seen in Figure 4, the inclusion of the \mathcal{L}_{NFL-BA} loss reduces the amount of artifacts, is able to more accurately render the shading of the scene, and preserves geometric structures with more details

than its original photometric bundle adjustment counterpart. Additionally, the resulting point clouds shown in Figures 7 and 8, are more complete and consistent with the true structure on the colon when our loss is incorporated into training. This suggests that the loss function effectively compensates for depth inaccuracies by optimizing the alignment of features under varying lighting conditions and minimizing photometric inconsistencies.

In the no-depth initialization setting, the improvement with \mathcal{L}_{NFL-BA} is only marginal for tracking, suggesting that the absence of depth information may limit the effectiveness of \mathcal{L}_{NFL-BA} in enhancing accuracy. Although it can successfully estimate camera pose (Figs. 7 and 8) and render plausible reconstructions, the resulting point clouds are generally too sparse to capture any meaningful geometric shape and details (Figs. 7 and 8). This is because the optimized 3D Gaussians are relatively wider capturing textureless tissue surfaces without having geometric details, which helps in reducing rendering and tracking loss but results in poor point cloud reconstruction. Incorporating \mathcal{L}_{NFL-BA} aids in densifying these point clouds, allowing for a richer spatial representation that enhances the network’s ability to capture geometric details in scenes where depth cues are otherwise lacking.

4.3. Improving EndoGSLAM with NFL-BA

While EndoGSLAM demonstrates robust baseline performance, particularly with ground truth depth data, our results show that the addition of \mathcal{L}_{NFL-BA} yields substantial improvements in tracking accuracy, with some improvement in mapping fidelity and rendering quality as well. These improvements are especially apparent in scenarios where only noisy depth data is available, as is typically the case in real endoscopic procedures.

Tracking. In terms of tracking accuracy, EndoGSLAM performs reliably with oracle depth indicating that EndoGSLAM’s photometric and geometric bundle adjustment can already estimate camera pose fairly accurately when high-quality depth information

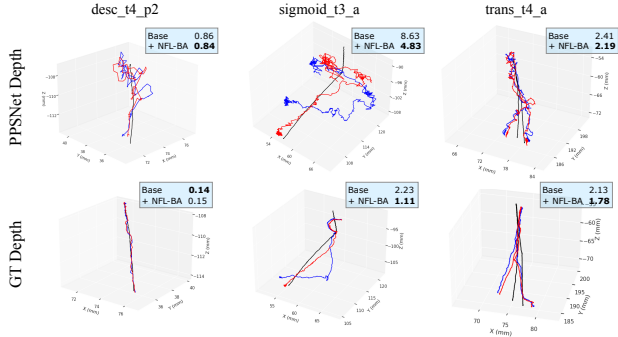


Figure 5. Camera tracking improvement over EndoGS [53]. We show that the proposed NFL-BA loss (in blue) improves the tracking of the baseline SLAM algorithm, EndoGS (in red), for 3 sequences for different depth initialization. Average tracking error ATE_t for each sequence is reported in the inset (zoom for details).

is available. When applied with ground truth depth, \mathcal{L}_{NFL-BA} achieves modest 8% improvement; though small, this confirms that \mathcal{L}_{NFL-BA} enhances tracking accuracy even under ideal depth conditions. However, when switching to estimated depth maps from PPSNet, tracking accuracy declines significantly, by 88% degradation in ATE_t , due to the noise inherent in the estimated data. The presence of \mathcal{L}_{NFL-BA} improves the tracking accuracy on average by 22% with PPSNet depth, resulting in more accurate trajectory as shown in Figure 6, especially noticeable for ‘sigmoid.t3.a’. Similarly to MonoGS, the improvement in tracking accuracy under noisy conditions underscores \mathcal{L}_{NFL-BA} ’s ability to mitigate the effects of depth noise.

Mapping. Similarly to the results of MonoGS, we see more dense point cloud Figs. 8 and 10. While the improvement in Chamfer distance is not as pronounced as with MonoGS, the proposed loss \mathcal{L}_{NFL-BA} improves the robustness of mapping.

Rendering. The integration of \mathcal{L}_{NFL-BA} also yields perceptual benefits in rendering quality. \mathcal{L}_{NFL-BA} helps to suppress noise and correct intensity inconsistencies that can arise from near-field lighting effects, leading to more visually coherent reconstructions. Additionally, the addition of our loss leads to more complete reconstructions and renderings as seen in Fig. 6. While the improvement is small in the oracle depth setting, the proposed loss \mathcal{L}_{NFL-BA} reinforces the robustness in maintaining image fidelity across both ideal and noisy depth inputs.

4.4. Ablation Study

As our proposed NFL-BA loss can be used for both tracking and mapping phase, we separately add the loss term in each phase to analyze performance boost in each stage (Table 2). We found that in the monocular setting, using the mapping only setting yielded the best tracking results but when there is a depth input, using our loss in both tracking and the mapping yields the best tracking and rendering results. When ground truth depth is available, adding \mathcal{L}_{NFL-BA} to the mapping phase is sufficient for improving trajectory; however, when there is only noisy or estimated depth, incorporating our loss term into tracking is more effective. Additionally we noticed that down the barrel sequences saw the most benefits from the addition of \mathcal{L}_{NFL-BA} .

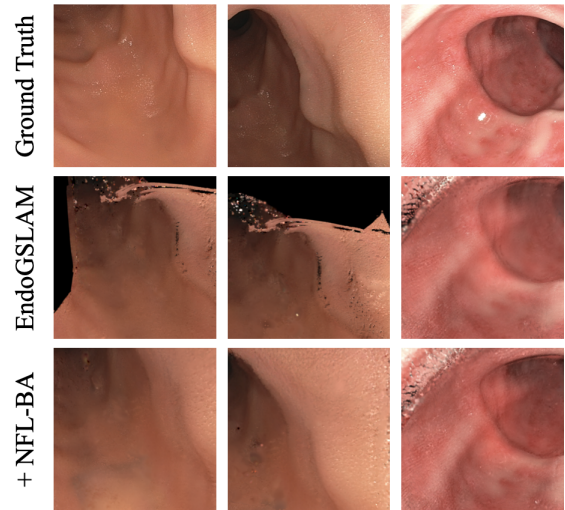


Figure 6. Rendered images from EndoGSLAM. Adding NFL-BA loss leads to more accurate shape and provides better coverage.

| Track. | Map. | No Depth | | PPSNet Depth | | GT Depth | |
|--------|------|-------------|--------------|--------------|--------------|-------------|--------------|
| | | ATE_t | PSNR | ATE_t | PSNR | ATE_t | PSNR |
| | | 2.33 | 18.78 | 3.72 | 10.41 | 3.20 | 19.73 |
| ✓ | | 3.21 | 19.10 | 2.41 | 19.89 | 3.14 | 20.61 |
| | ✓ | 2.31 | 18.80 | 3.06 | 19.17 | 1.98 | 19.36 |
| ✓ | ✓ | 2.97 | 19.89 | 2.40 | 20.60 | 1.72 | 19.55 |

Table 2. Importance of NFL-BA loss in both tracking and mapping phase, evaluated with MonoGS [24].

5. Conclusions

In this paper, we introduce a novel bundle adjustment loss that uses light intensity fall-off based on the relative distance and orientation between the surface and the co-located light and camera to optimize camera pose and surface representation. This loss function is especially effective for endoscopic SLAM systems, which face challenging dynamic near-field lighting conditions with textureless surfaces and specular highlights, where traditional geometric or photometric bundle adjustment losses perform poorly. While our idea is general, we formulate this Near-Field Light Bundle Adjustment for 3D Gaussian surface representation-based SLAM systems, which has recently proved to be effective for textureless surfaces and are highly efficient. We then modified two state-of-the-art 3D Gaussian SLAMs, MonoGS and EndoGSLAM, by adding the NFL-BA strategies for them. We show that our proposed bundle adjustment loss significantly improves camera tracking and mapping performance for both SLAM frameworks and is able to generate accurate and realistic 3D point clouds, novel-view rendering, and camera tracking for many challenging sequences.

Acknowledgment

This work is supported by a National Institute of Health (NIH) project #1R21EB035832 “Next-gen 3D Modeling of Endoscopy Videos”.

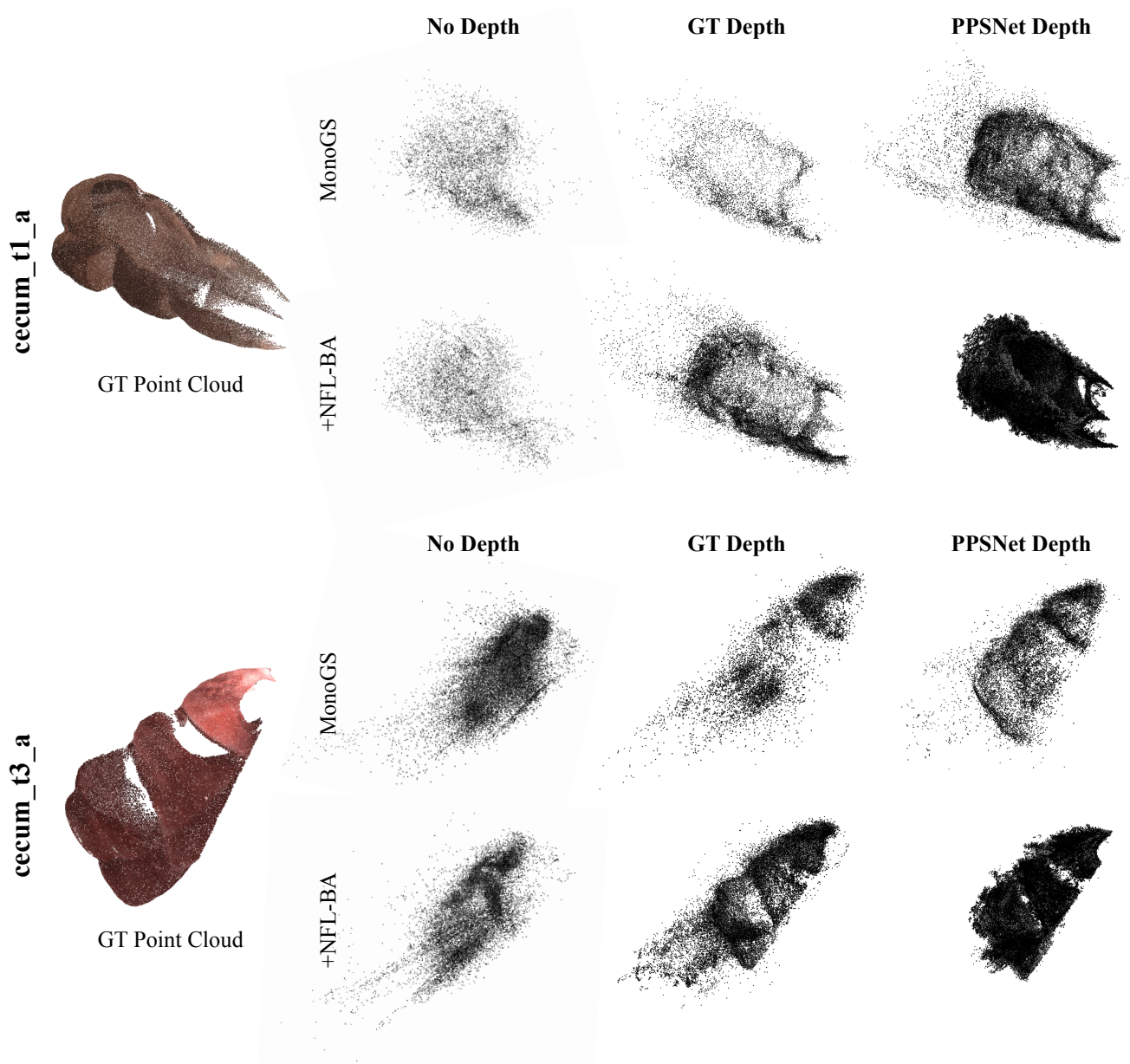


Figure 7. **MonoGS Point Clouds Part 1:** We compared the pointclouds for 3 depth settings – no depth, ground truth, and PPSNET — with and without our proposed loss on cecum_t1_a and cecum_t3_a. Although monoGS without depth information demonstrates strong tracking and rendering performance, the resulting point clouds are too sparse and scattered to form a meaningful geometric structure. In contrast, incorporating our loss results in a **denser point cloud**, as illustrated in 8. Furthermore, when using noisy depth inputs (e.g., PPSNet depth), our loss effectively **reduces scattering** caused by ambiguous depth data, enhancing the overall structure.

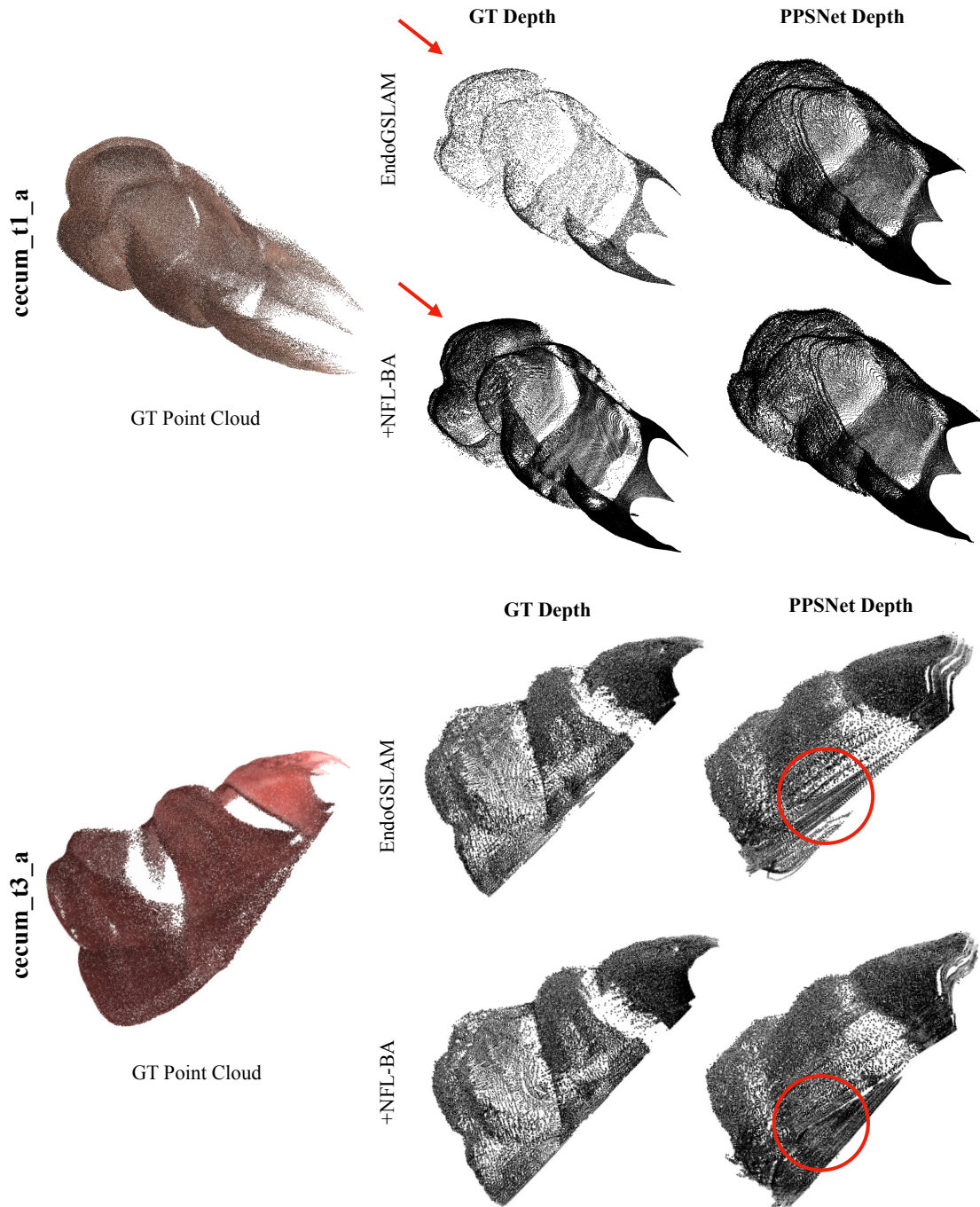


Figure 8. **EndoGSLAM Point Clouds** Part 1: We compared the pointclouds for 2 depth settings – ground truth and PPSNET — with and without our proposed loss on `cecum_t1_a` and `cecum_t3_a`. We found that the addition of \mathcal{L}_{NFL-BA} leads to a **more dense point cloud** and minimized gaps.

References

- [1] Hatem Alismail, Brett Browning, and Simon Lucey. Photometric bundle adjustment for vision-based slam, 2016. 3
- [2] Taylor L Bobrow, Mayank Golhar, Rohan Vijayan, Venkata S Akshintala, Juan R Garcia, and Nicholas J Durr. Colonoscopy 3d video dataset with paired depth from 2d-3d registration. *Medical Image Analysis*, page 102956, 2023. 2, 5, 6
- [3] C. Campos, R. Elvira, J. J. G. Rodríguez, J. M. M. Montiel, and J. D. Tardós. Orb-slam3: An accurate open-source library for visual, visual-inertial, and multi-map slam. *IEEE Transactions on Robotics*, 37(6):1874–1890, 2021. 2
- [4] Devendra Singh Chaplot, Ruslan Salakhutdinov, Abhinav Gupta, and Saurabh Gupta. Neural topological slam for visual navigation. In *Proceedings of the IEEE/CVF conference on computer vision and pattern recognition*, pages 12875–12884, 2020. 1
- [5] Hanlin Chen, Fangyin Wei, Chen Li, Tianxin Huang, Yunsong Wang, and Gim Hee Lee. Vcr-gaus: View consistent depth-normal regularizer for gaussian surface reconstruction. *arXiv preprint arXiv:2406.05774*, 2024. 4
- [6] T. Collins and A. Bartoli. Towards live dense reconstruction in minimally invasive surgery and its application to augmented reality. *Medical Image Analysis*, 27:1–11, 2016. 2
- [7] B. Cui, H. Zhang, X. Li, W. Zhou, and T. Cheng. Endodac: Efficient adapting foundation model for self-supervised depth estimation from any endoscopic camera. In *Proceedings of the Medical Image Computing and Computer-Assisted Intervention Conference (MICCAI)*, 2024. 2
- [8] Tianchen Deng, Yaohui Chen, Leyan Zhang, Jianfei Yang, Shenghai Yuan, Jiuming Liu, Danwei Wang, Hesheng Wang, and Weidong Chen. Compact 3d gaussian splatting for dense visual slam, 2024. 2
- [9] Z. Dong, R. Isidro, and D. Stoyanov. Real-time monocular slam using natural features in endoscopic images. In *Medical Image Computing and Computer-Assisted Intervention (MICCAI)*, pages 584–591, 2014. 2
- [10] J. Engel, V. Koltun, and D. Cremers. Direct sparse odometry. *IEEE Transactions on Pattern Analysis and Machine Intelligence*, 40(3):611–625, 2018. 2, 3
- [11] Juan J Gómez-Rodríguez, José Lamarca, Javier Morlana, Juan D Tardós, and José MM Montiel. Sd-defslam: Semi-direct monocular slam for deformable and intracorporeal scenes. In *2021 IEEE international conference on robotics and automation (ICRA)*, pages 5170–5177. IEEE, 2021. 2
- [12] Jiaxin Guo, Jiangliu Wang, Di Kang, Wenzhen Dong, Wenting Wang, and Yun-hui Liu. Free-SurGS: SfM-Free 3D Gaussian Splatting for Surgical Scene Reconstruction. In *proceedings of Medical Image Computing and Computer Assisted Intervention – MICCAI 2024*. Springer Nature Switzerland, 2024. 2
- [13] R. Hartley and A. Zisserman. *Multiple View Geometry in Computer Vision*. Cambridge University Press, 2003. 3
- [14] Michel Hayoz, Christopher Hahne, Thomas Kurmann, Max Allan, Guido Beldi, Daniel Candinas, Pablo Márquez-Neila, and Raphael Sznitman. Online 3D reconstruction and dense tracking in endoscopic videos. In *proceedings of Medical Image Computing and Computer Assisted Intervention – MICCAI 2024*. Springer Nature Switzerland, 2024. 2
- [15] Huajian Huang, Longwei Li, Cheng Hui, and Sai-Kit Yeung. Photo-slam: Real-time simultaneous localization and photo-realistic mapping for monocular, stereo, and rgb-d cameras. In *Proceedings of the IEEE/CVF Conference on Computer Vision and Pattern Recognition*, 2024. 1, 2
- [16] Yiming Huang, Beilei Cui, Long Bai, Ziqi Guo, Mengya Xu, Mobarakol Islam, and Hongliang Ren. Endo-4DGS: Endoscopic Monocular Scene Reconstruction with 4D Gaussian Splatting. In *proceedings of Medical Image Computing and Computer Assisted Intervention – MICCAI 2024*. Springer Nature Switzerland, 2024. 2
- [17] Y. Iwahori, H. Sugie, and N. Ishii. Reconstructing shape from shading images under point light source illumination. In *[1990] Proceedings. 10th International Conference on Pattern Recognition*, pages 83–87 vol.1, 1990. 4
- [18] Bernhard Kerbl, Georgios Kopanas, Thomas Leimkuehler, and George Drettakis. 3d gaussian splatting for real-time radiance field rendering. *ACM Trans. Graph.*, 42(4), 2023. 1, 2, 3
- [19] C. Kerl, J. Sturm, and D. Cremers. Dense visual slam for rgb-d cameras. In *IEEE/RSJ International Conference on Intelligent Robots and Systems (IROS)*, pages 2100–2106, 2013. 2
- [20] C. Lichy and Other authors. Photometric stereo with near-field lighting using neural networks. In *Proceedings of the IEEE Conference on Computer Vision and Pattern Recognition*, pages zz–aa, 2022. 3
- [21] Daniel Lichy, Soumyadip Sengupta, and David W. Jacobs. Fast light-weight near-field photometric stereo. In *Proceedings of the IEEE/CVF Conference on Computer Vision and Pattern Recognition (CVPR)*, pages 12612–12621, 2022. 3, 5
- [22] Hengyu Liu, Yifan Liu, Chenxin Li, Wuyang Li, and Yixuan Yuan. Lgs: A light-weight 4d gaussian splatting for efficient surgical scene reconstruction. In *proceedings of Medical Image Computing and Computer Assisted Intervention – MICCAI 2024*. Springer Nature Switzerland, 2024. 2
- [23] Yifan Liu, Chenxin Li, Chen Yang, and Yixuan Yuan. Endogaussian: Gaussian splatting for deformable surgical scene reconstruction. *arXiv preprint arXiv:2401.12561*, 2024. 2
- [24] J. Lu, Y. Zhang, and X. Chen. Monogs: Monocular gaussian splatting for robust slam. In *Proceedings of the IEEE International Conference on Robotics and Automation (ICRA)*, 2023. 2, 4, 6, 8
- [25] Ruibin Ma, Rui Wang, Stephen Pizer, Julian Rosenman, Sarah K McGill, and Jan-Michael Frahm. Real-time 3d reconstruction of colonoscopic surfaces for determining missing regions. In *Medical Image Computing and Computer Assisted Intervention–MICCAI 2019: 22nd International Conference, Shenzhen, China, October 13–17, 2019, Proceedings, Part V 22*, pages 573–582. Springer, 2019. 2
- [26] Hidenobu Matsuki, Riku Murai, Paul H.J. Kelly, and Andrew J. Davison. Gaussian splatting slam. In *Proceedings of the IEEE/CVF Conference on Computer Vision and Pattern Recognition (CVPR)*, pages 18039–18048, 2024. 1, 2, 3, 6

- [27] R. Mur-Artal, J. M. M. Montiel, and J. D. Tardos. Orb-slam: A versatile and accurate monocular slam system. In *IEEE Transactions on Robotics*, pages 1147–1163, 2015. 2
- [28] Andriy Myronenko and Xubo Song. Point set registration: Coherent point drift. *IEEE Transactions on Pattern Analysis and Machine Intelligence*, 32(12):2262–2275, 2010. 6
- [29] Kutsev Bengisu Ozyoruk, Guliz Irem Gokceler, Taylor L. Bobrow, Gulfize Coskun, Kagan Incetan, Yasin Almalioglu, Faisal Mahmood, Eva Curto, Luis Perdigoto, Marina Oliveira, Hasan Sahin, Helder Araujo, Henrique Alexandrino, Nicholas J. Durr, Hunter B. Gilbert, and Mehmet Turan. Endoslam dataset and an unsupervised monocular visual odometry and depth estimation approach for endoscopic videos. *Medical Image Analysis*, 71:102058, 2021. 2
- [30] Albert Palomer, Pere Ridao, and David Ribas. Inspection of an underwater structure using point-cloud slam with an auv and a laser scanner. *Journal of field robotics*, 36(8):1333–1344, 2019. 1
- [31] Akshay Paruchuri, Samuel Ehrenstein, Shuxian Wang, Inbar Fried, Stephen M Pizer, Marc Niethammer, and Roni Sengupta. Leveraging near-field lighting for monocular depth estimation from endoscopy videos. In *Computer Vision – ECCV 2024*, Cham, 2024. Springer Nature Switzerland. 2, 3, 4, 5, 6, 1
- [32] Erik Sandström, Yue Li, Luc Van Gool, and Martin R Oswald. Point-slam: Dense neural point cloud-based slam. In *Proceedings of the IEEE/CVF International Conference on Computer Vision*, pages 18433–18444, 2023. 1
- [33] C. Shen, H. Wang, and F. Zhao. Gs-slam: Gaussian splatting for high-quality slam. In *Proceedings of the IEEE Conference on Computer Vision and Pattern Recognition*, 2023. 2, 6
- [34] Yufei Shi, Beijia Lu, Jia-Wei Liu, Ming Li, and Mike Zheng Shou. Colonerf: Neural radiance fields for high-fidelity long-sequence colonoscopy reconstruction. *arXiv preprint arXiv:2312.02015*, 2023. 2
- [35] Jingwei Song. *3D non-rigid SLAM in minimally invasive surgery*. PhD thesis, 2020. 2
- [36] Xuanshuang Tang, Haisu Tao, Yinling Qian, Jian Yang, Ziliang Feng, and Qiong Wang. Real-time deformable slam with geometrically adapted template for dynamic monocular laparoscopic scenes. *International Journal of Computer Assisted Radiology and Surgery*, pages 1–9, 2024. 2
- [37] Z. Teed and J. Deng. Droid-slam: Deep visual slam for monocular, stereo, and rgb-d cameras. In *Proceedings of the IEEE/CVF Conference on Computer Vision and Pattern Recognition*, pages 16578–16587, 2021. 2
- [38] Fabio Tosi, Youmin Zhang, Ziren Gong, Erik Sandström, Stefano Mattocchia, Martin R Oswald, and Matteo Poggi. How nerfs and 3d gaussian splatting are reshaping slam: a survey. *arXiv preprint arXiv:2402.13255*, 4, 2024. 4
- [39] Shimon Ullman. The interpretation of structure from motion. *Proceedings of the Royal Society of London. Series B. Biological Sciences*, 203(1153):405–426, 1979. 3
- [40] Kailing Wang, Chen Yang, Yuehao Wang, Sikuang Li, Yan Wang, Qi Dou, Xiaokang Yang, and Wei Shen. EndoGSLAM: Real-Time Dense Reconstruction and Tracking in Endoscopic Surgeries using Gaussian Splatting . In *proceedings of Medical Image Computing and Computer Assisted Intervention – MICCAI 2024*. Springer Nature Switzerland, 2024. 2
- [41] Shuxian Wang, Yubo Zhang, Sarah K. McGill, Julian G. Rosenman, Jan-Michael Frahm, Soumyadip Sengupta, and Stephen M. Pizer. A surface-normal based neural framework for colonoscopy reconstruction. In *Information Processing in Medical Imaging*, pages 797–809, Cham, 2023. Springer Nature Switzerland. 6
- [42] Shuxian Wang, Yubo Zhang, Sarah K McGill, Julian G Rosenman, Jan-Michael Frahm, Soumyadip Sengupta, and Stephen M Pizer. A surface-normal based neural framework for colonoscopy reconstruction. In *International Conference on Information Processing in Medical Imaging*, pages 797–809. Springer, 2023. 2
- [43] Yuehao Wang, Yonghao Long, Siu Hin Fan, and Qi Dou. Neural rendering for stereo 3d reconstruction of deformable tissues in robotic surgery. In *International Conference on Medical Image Computing and Computer-Assisted Intervention*, pages 431–441. Springer, 2022. 2
- [44] Qianyi Wu, Jianmin Zheng, and Jianfei Cai. Surface reconstruction from 3d gaussian splatting via local structural hints. In *Computer Vision – ECCV 2024*, Cham, 2024. Springer Nature Switzerland. 4
- [45] Chi Yan, Delin Qu, Dan Xu, Bin Zhao, Zhigang Wang, Dong Wang, and Xuelong Li. Gs-slam: Dense visual slam with 3d gaussian splatting. In *Proceedings of the IEEE/CVF Conference on Computer Vision and Pattern Recognition*, pages 19595–19604, 2024. 1, 2, 4
- [46] Chen Yang, Kailing Wang, Yuehao Wang, Xiaokang Yang, and Wei Shen. Neural lerplane representations for fast 4d reconstruction of deformable tissues. In *Medical Image Computing and Computer Assisted Intervention – MICCAI 2023*, pages 46–56, Cham, 2023. Springer Nature Switzerland. 2
- [47] Lihe Yang, Bingyi Kang, Zilong Huang, Zhen Zhao, Xiaogang Xu, Jiashi Feng, and Hengshuang Zhao. Depth anything v2. *arXiv:2406.09414*, 2024. 5, 6
- [48] Shuojue Yang, Qian Li, Daiyun Shen, Bingchen Gong, Qi Dou, and Yueming Jin. Deform3DGS: Flexible Deformation for Fast Surgical Scene Reconstruction with Gaussian Splatting . In *proceedings of Medical Image Computing and Computer Assisted Intervention – MICCAI 2024*. Springer Nature Switzerland, 2024. 2
- [49] Keyang Ye, Qiming Hou, and Kun Zhou. 3d gaussian splatting with deferred reflection. In *ACM SIGGRAPH 2024 Conference Papers*, New York, NY, USA, 2024. Association for Computing Machinery. 4
- [50] Vladimir Yugay, Yue Li, Theo Gevers, and Martin R. Oswald. Gaussian-slam: Photo-realistic dense slam with gaussian splatting, 2024. 2
- [51] Carlton Zdanski, Stephanie Davis, Yi Hong, Di Miao, Cory Quammen, Sorin Mitran, Brad Davis, Marc Niethammer, Julia Kimbell, Elizabeth Pitkin, Jason Fine, Lynn Fordham, Brad Vaughn, and Richard Superfine. Quantitative assessment of the upper airway in infants and children with subglottic stenosis. *The Laryngoscope*, 126, 2015. 2
- [52] Ruyi Zha, Xuelian Cheng, Hongdong Li, Mehrtash Harandi, and Zongyuan Ge. Endosurf: Neural surface reconstruction

- of deformable tissues with stereo endoscope videos. In *Medical Image Computing and Computer Assisted Intervention – MICCAI 2023: 26th International Conference, Vancouver, BC, Canada, October 8–12, 2023, Proceedings, Part IX*, page 13–23, Berlin, Heidelberg, 2023. Springer-Verlag. [2](#)
- [53] M. Zhang, F. Wu, Y. Zhang, L. Chen, and Q. Li. Endogslam: Real-time dense reconstruction and tracking in endoscopic surgeries. In *Proceedings of the Medical Image Computing and Computer-Assisted Intervention Conference (MICCAI)*, 2024. [2](#), [3](#), [6](#), [8](#)
- [54] Richard Zhang, Phillip Isola, Alexei A. Efros, Eli Shechtman, and Oliver Wang. The unreasonable effectiveness of deep features as a perceptual metric. In *Proceedings of the IEEE Conference on Computer Vision and Pattern Recognition (CVPR)*, 2018. [6](#)
- [55] Yubo Zhang, Jan-Michael Frahm, Samuel Ehrenstein, Sarah K McGill, Julian G Rosenman, Shuxian Wang, and Stephen M Pizer. Colde: a depth estimation framework for colonoscopy reconstruction. *arXiv preprint arXiv:2111.10371*, 2021. [2](#)
- [56] S. Zhi, J. Lai, A. Kundu, M. Bloesch, A. Davison, and A. Zisserman. Nerf-slam: Real-time dense monocular slam with neural radiance fields. In *Proceedings of the European Conference on Computer Vision (ECCV)*, 2022. [1](#)
- [57] L. Zhou, R. Klette, and K. Scheibe. A multi-image shape-from-shading framework for near-lighting perspective endoscopes. *International Journal of Computer Vision*, 82:1–24, 2009. [3](#)
- [58] Z. Zhou, Y. Li, and N. Snavely. Deep bundle adjustment for robust visual slam. In *IEEE Conference on Computer Vision and Pattern Recognition*, pages 13465–13474, 2020. [3](#)
- [59] A. Zhu, Z. Zhang, H. Su, L. Li, G. Wang, and X. Li. Nicerslam: Neural implicit scalable encoding with monocular depth and normal priors. In *Proceedings of the IEEE/CVF Conference on Computer Vision and Pattern Recognition (CVPR)*, 2023. [1](#)
- [60] Z. Zhu, T. Yu, X. Zhang, J. Li, Y. Zhang, and Y. Fu. Nicerslam: Neural implicit scalable encoding for slam. In *Proceedings of the IEEE Conference on Computer Vision and Pattern Recognition*, 2021. [2](#)
- [61] Zihan Zhu, Songyou Peng, Viktor Larsson, Weiwei Xu, Hujun Bao, Zhaopeng Cui, Martin R. Oswald, and Marc Pollefeys. Nice-slam: Neural implicit scalable encoding for slam. In *Proceedings of the IEEE/CVF Conference on Computer Vision and Pattern Recognition (CVPR)*, 2022. [1](#)
- [62] Z. Zhu, T. Yu, X. Zhang, J. Li, Y. Zhang, and Y. Fu. Neuralrgb-d: Neural representations for depth estimation and scene mapping. In *Proceedings of the IEEE Conference on Computer Vision and Pattern Recognition*, 2022. [2](#)

NFL-BA: Improving Endoscopic SLA M with Near-Field Light Bundle Adjustmen

Supplementary Material

A. Overview of Appendices

Our appendices contain the following additional details:

- Appendix B provides implementation details of our experimental settings.
- In Appendix C, we present per-sequence qualitative evaluation of tracking and mapping.

B. Implementation Details

Dataset As mentioned in the main paper, we use eight test sequences of the monocular endoscopy depth estimation method, PPSNet [31]. These sequences cover various anatomical structures and camera movements. The names of the sequences are as follows: cecum_t1_a, cecum_t2_a, cecum_t3_a, sigmoid_t3_a, desc_t4_a_p2, trans_t2_a, trans_t3_a, and trans_t4_a.

Preprocessing In our experiments, we use downscaled and cropped images. Specifically, we resize each image to have a height of 384 pixels while maintaining the aspect ratio, then crop the central region to obtain a 384×384 pixel image.

C. Per-Sequence Results

Figures 11 and 12 illustrate trajectories of MonoGS and EndoGSLAM with and without the proposed bundle adjustment loss.

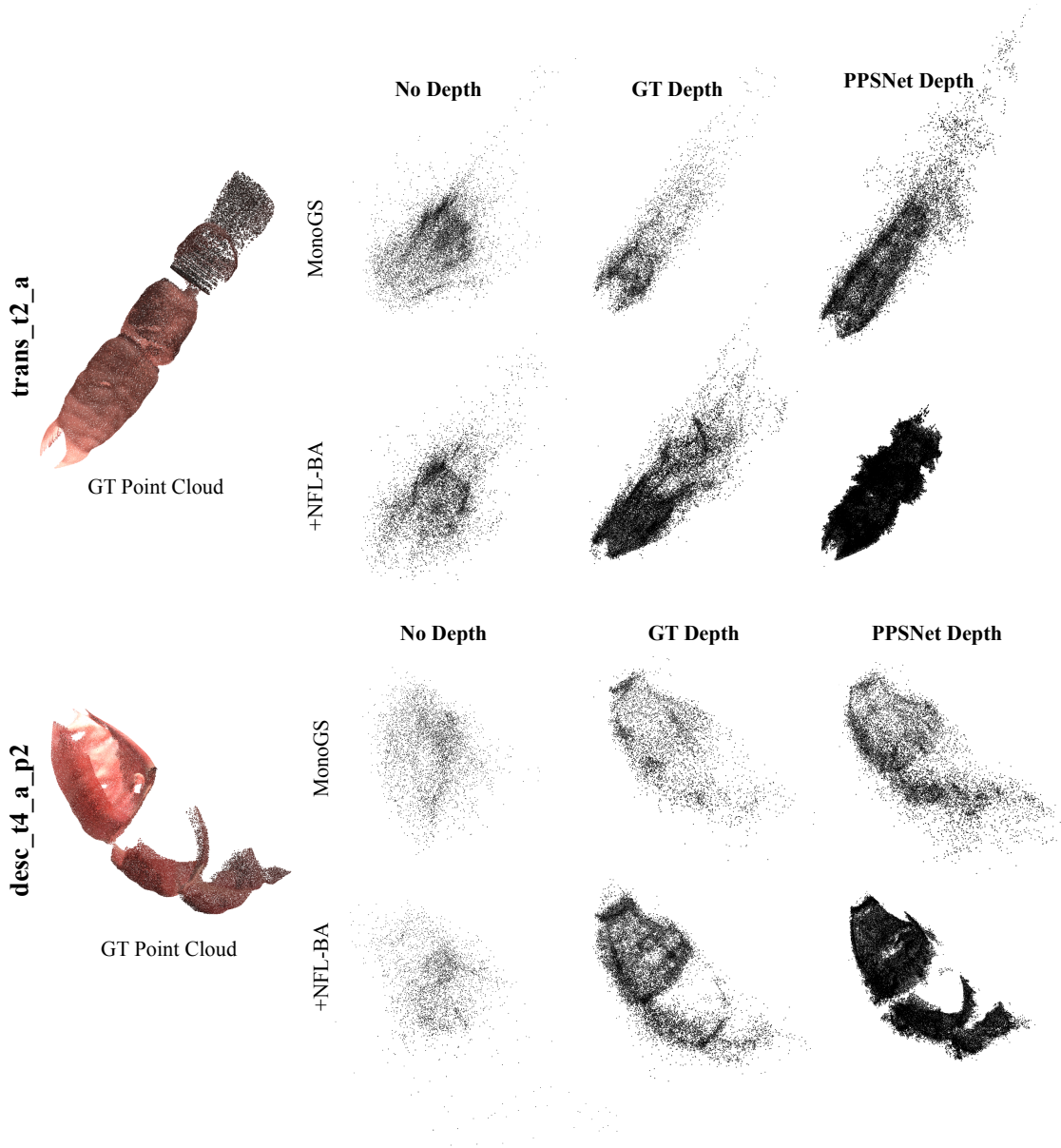


Figure 9. **MonoGS Point Clouds Part 2:** Once again, we observe sparse point clouds in the no-depth initialization scenario. In the ground truth depth case, for both `trans_t2_a` and `desc_t4_a_p2`, the inclusion of our term enables the capture of more distant structures, particularly **along ridges**. Similarly to Fig. 7, the PPSNet case demonstrates a significant reduction in scattering.

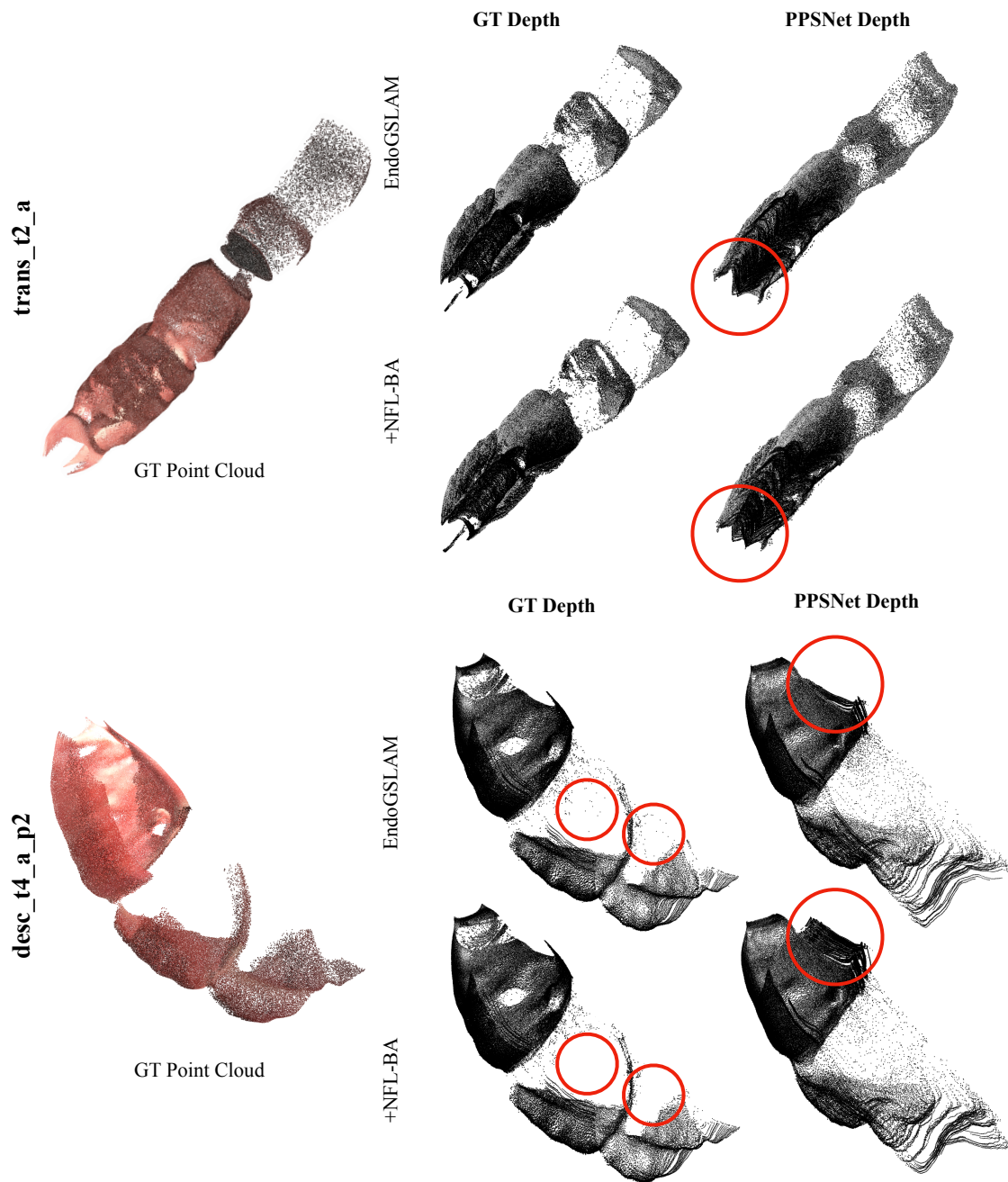


Figure 10. **EndoGSLAM Point Clouds Part 2:** Similarly to Fig. 8, we compared the pointclouds for 2 depth settings – ground truth and PPSNET — with and without our proposed loss on trans.t2.a and desc.t4.a.p2. Here, we see that, especially in the PPSNET depth setting, by incorporating \mathcal{L}_{NFL-BA} , the **geometry of the point clouds is refined**, enabling the capture of subtle structures near edges and resulting in a more comprehensive representation.

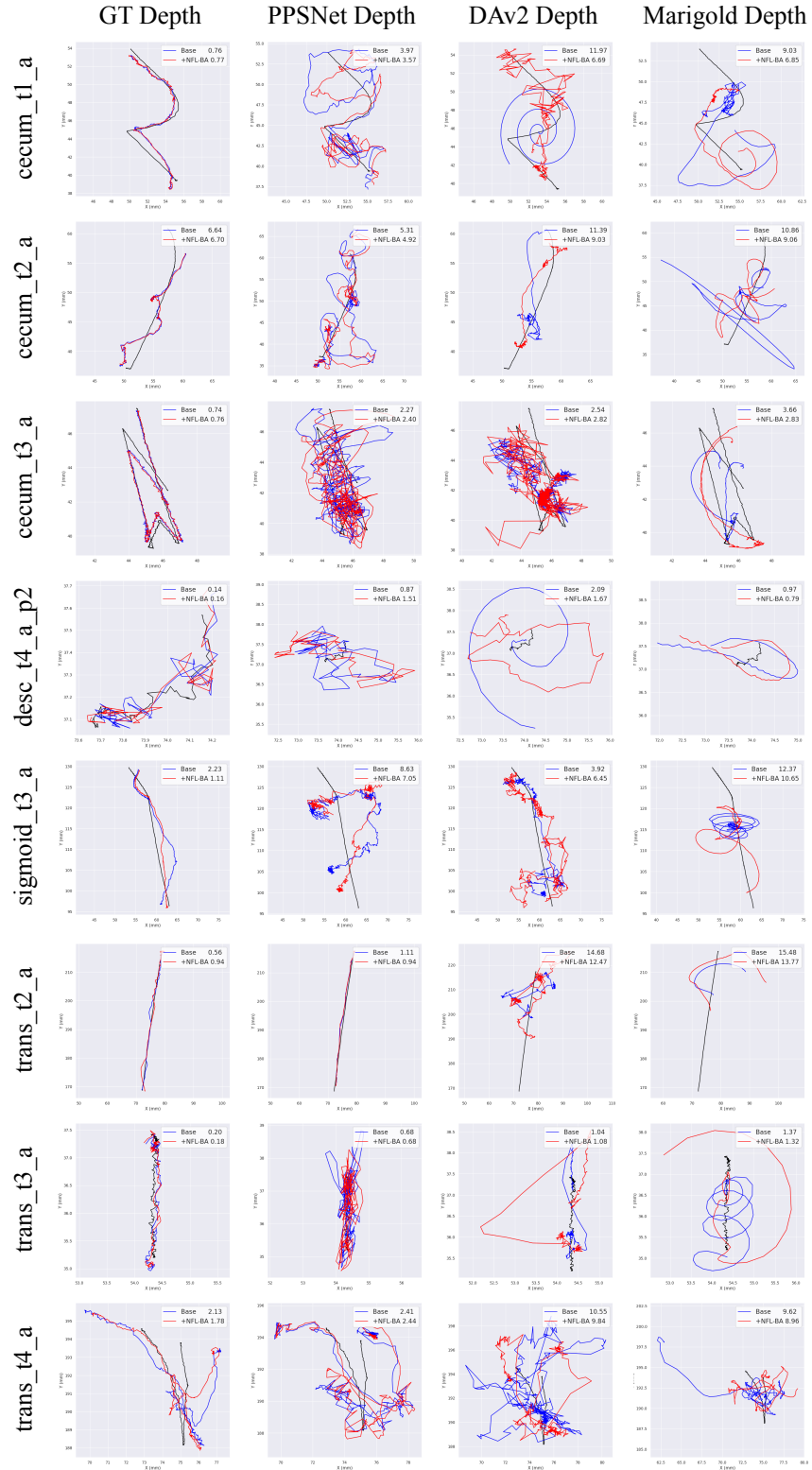


Figure 11. **Camera tracking improvement over EndoGS.** We show that the proposed NFL-BA loss (in blue) improves the tracking of the baseline SLAM algorithm, EndoGS (in red), for all for different depth initialization. Average tracking error ATE_t for each sequence is reported in the inset. DepthAnything Depth and Marigold depth both lead to poor tracking. The addition of our loss tends to **smoothen the trajectory**.

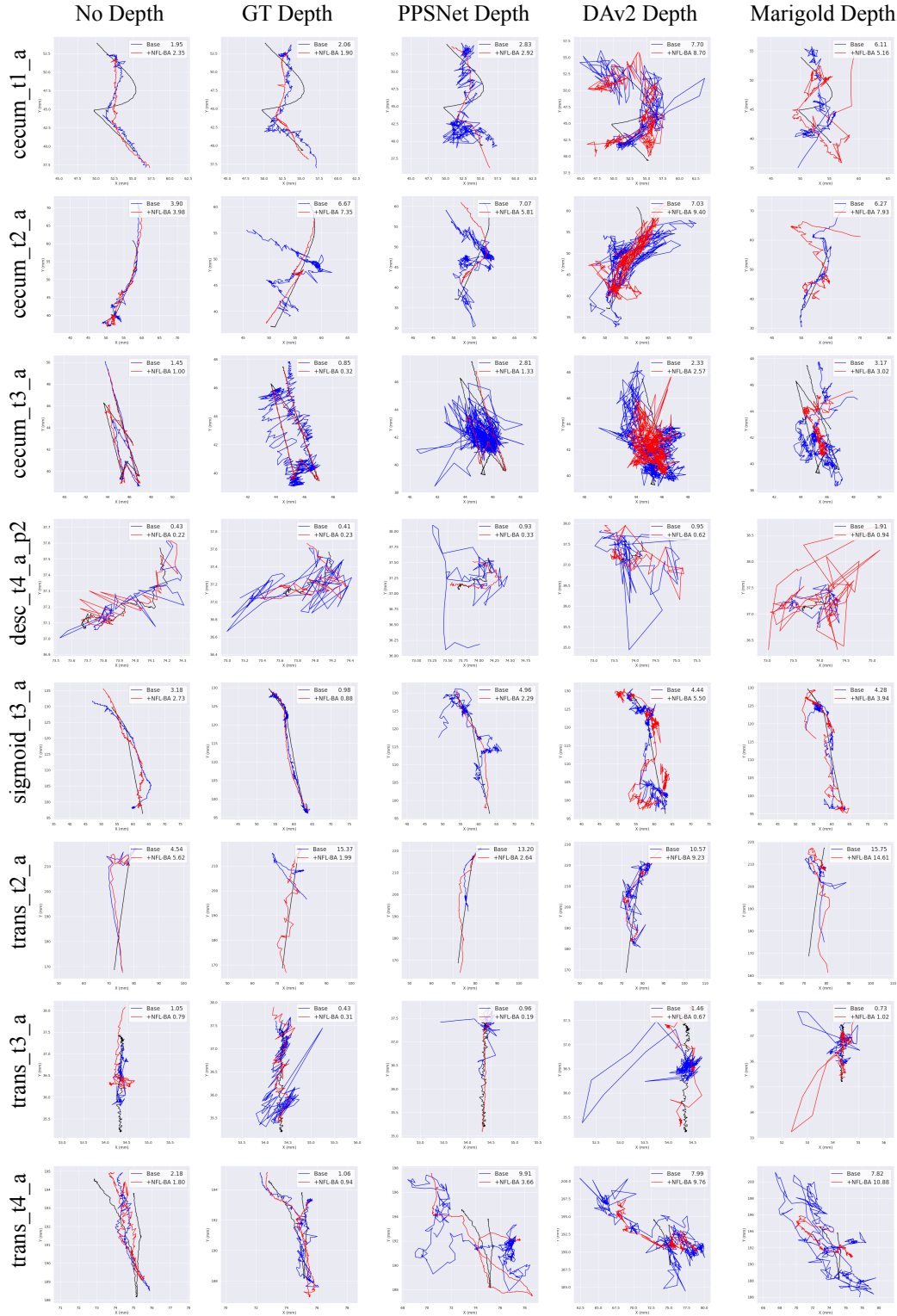


Figure 12. **Camera tracking improvement over MonoGS.** We show that the proposed NFL-BA loss (in blue) improves the tracking of the baseline SLAM, MonoGS algorithm (in red), for all for different depth initialization. Average tracking error ATE_t for each sequence is reported in the inset. When the baseline performs poorly, the addition of our term tends to reduce the noise proved by the depth but is not always able to completely recover.